Biofidelity Evaluation of GHBMC Male Occupant Models in Rear Impacts

Maika Katagiri, Jay Zhao, Sungwoo Lee, Kevin Moorhouse and Yun-Seok Kang

Abstract Historically, the rear-impact mode has received most attention in the context of low-speed rear-end crashes, but in the future of automated vehicles (AV), the rear-impact mode may occur at higher speed in frontal crashes with a rearward-facing seating configuration. While the use of human body models (HBM) in virtual testing for AV is expected, current HBMs have never been validated in moderate/high-speed rear impacts. The objective of this study is to evaluate the biofidelity of the Global Human Body Models Consortium average male occupant detailed and simplified HBMs by using biomechanical targets generated from a series of post mortem human surrogates rear-impact tests at two severities (17 km/h; 24 km/h) with an experimental sled system, which mimics the dynamic characteristics of a modern vehicle seatback. The NHTSA Biofidelity Ranking System was used to evaluate the HBMs. The HBMs exhibited better biofidelity 1) at 17 km/h than 24 km/h, and 2) in the head to T1 region, which is relevant to rear-impact-related injuries, than the T1 to pelvis region. The detailed HBM received a better biofidelity score than the simplified HBM in every studied component. Limitations for the HBMs' biofidelity were indicated in the modelling of their spines and surrounding flesh.

Keywords Biofidelity, Experimental sled system, Human body model, Post mortem human subject, Rear impact.

I. INTRODUCTION

Recently, the rearward-facing seating configuration has been more heavily considered with automated vehicles, especially for longer journeys [1]. Historically, the rear-impact mode has been addressed in the low-speed rear-end crash mode, where cervical spine injuries (e.g. whiplash) commonly occur [2]. However, with rearward-facing seats, the rear-impact mode may happen in frontal collisions, which generally occur at higher severities than rear-end collisions. Consequently, severe and unexpected injuries in the rear-impact mode may occur more frequently than at present.

It is expected that human body models (HBM) will be part of virtual testing to evaluate the crashworthiness of automated vehicles [3], in which seating configurations and occupant postures can be more versatile than in conventional vehicles. The Global Human Body Models Consortium (GHBMC) HBMs have been validated extensively at both the body regional level and the full-body level, which consisted of nine impact modes: four frontal, two near-side, two far-side, and one far-side oblique. The rear-impact mode has been considered only in neck-regional validation with volunteers or post mortem human subjects (PMHS) tests at low-speed (below ΔV of 15 km/h) with a rigid seatback [4-5]. Other HBMs have been validated in the rear-impact mode at the full-body level, and the impact severities fall below ΔV of 10 km/h [6-7]. Looking at the future of mobility, these validations need to be carried out at higher speed.

Kang *et al.* [8] performed a set of rear-impact tests by subjecting eight PMHSs positioned in an experimental seat system to ΔV of 17 km/h (8.8 g) and 24 km/h (10.5 g) and created biomechanical targets for the biofidelity evaluation of anthropomorphic test devices (ATDs). While the lower severity was selected as the lower tolerance boundary of FMVSS 202a, the higher severity was determined as an intermediate between FMVSS 202a for head restraint system regulation (18 km/h) and FMVSS 301 for rear-impact barrier test regulation (30 km/h), which is usually regarded as a high-severity impact [9]. To our knowledge, the severity range in the tests has been the highest among available PMHS rear-impact tests. Additionally, the experimental seat system, which mimicked the seatback recliner mechanism of an average production seat, provided a more realistic test environment than

M. Katagiri (e-mail: Maika.Katagiri@joysonsafety.com; tel: +1-248-475-6760) is Development Engineer, J. Zhao is Technical Manager and S. Lee is Senior Product Engineer at Joyson Safety Systems in Auburn Hills, Michigan, USA. K. Moorhouse is Chief of the Applied Biomechanics Division at NHTSA's Vehicle Research and Test Center (VRTC) in East Liberty, Ohio, USA. Y. Kang is Assistant Professor in the Injury Biomechanics Research Center at The Ohio State University in Columbus, Ohio, USA.

using a rigid seat with a non-rotating seatback, while the repeatability and reproducibility of the seatback were maintained throughout the tests. Thus, the PMHS tests were selected as a first step to evaluate the GHBMC HBMs in the rear-impact mode.

The objective of this study was to evaluate the biofidelity of the GHBMC 50th percentile male occupant detailed and simplified models by using the biomechanical targets generated from the PMHS rear-impact sled tests. The detailed HBM is considered more biofidelic than the simplified HBM due to its anatomical accuracy and precision. The simplified HBM is numerically efficient, which made it practical in virtual testing and development. The biofidelity level of the HBM was quantitatively and objectively evaluated with the National Highway Traffic Safety Administration (NHTSA) Biofidelity Ranking System (BRS) [10], which has been used to evaluate Hybrid III 50th, BioRID II, and RID3D in the same sled system with the PMHS tests [11].

II. METHODS

A set of rear-impact simulations at two severities (17 km/h; 24 km/h) was performed with the GHBMC 50th percentile male occupant detailed and simplified HBMs. The impact pulse with duration of 250 ms, which was taken from the PMHS tests (Fig. A-1 in Appendix), was applied to the sled system model, while gravity was applied to the HBM throughout the simulation. Prior to the impact simulation, each HBM was positioned to have equivalent posture to the average initial posture of the PMHSs, then settled on the seat. The Ls-Dyna version 970 R9.2 was used as a finite element (FE) solver.

Sled System Model

The sled system model was developed to mimic the experimental sled system used in the PMHS tests. The experimental sled system was representative of a typical production seat with seat pan angle of 20 degrees, seatback angle of 25 degrees, and constant rotational stiffness of 65 N-m/deg at the seat pivot as reported in [12]. The sled system model consisted of a sled buck, seat frame, seat cushion foam, a spring-damper system, and a three-point seatbelt, as shown in Fig. 1. Uniaxial load cells were implemented to measure external loads on the head restraint, seatback and seat pan, with the polarities indicated in Fig. 1.

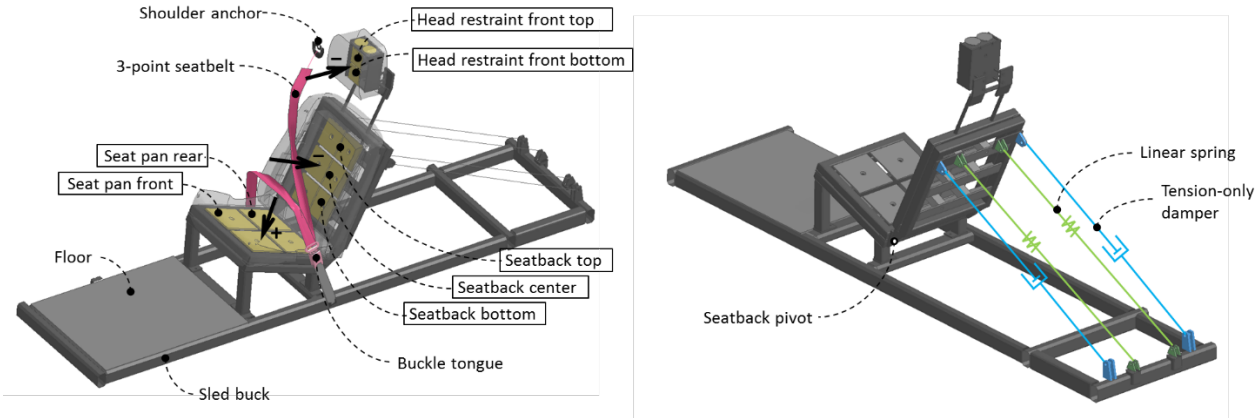

Fig. 1. The sled system model and the polarities of the uniaxial load cells (*left*) and the spring-damper system (*right*).

The geometry of the sled buck and the seat frame was taken from CAD data of the experimental sled system. Material properties of steel with density of 7800 kg/m^3 were used as rigid for the sled buck and frame. The geometry of the seat cushion foam was modified based on the 2012 Toyota Camry FE model developed by the National Crash Analysis Center, which was assumed to be close to that of a 1999 Toyota Camry seat cushion used in the tests. Material properties of low-density foam with densities of 50 kg/m^3 were used for the cushion foam of seatback and seat pan, and those with densities of 76.5 kg/m^3 were used for the head restraint. The total mass of the seatback including the frame and cushion foam was 30.0 kg, and that of the head restraint was 5.5 kg as in the tests.

The seatback reclining characteristic was defined as a spring-damper system. In the experimental sled system,

the seatback was connected to the seat pan via a pivot joint and supported with two springs and two one-way dampers. During the development of the experimental sled system for the PMHS tests [13], the stiffness value was determined by analysing data of seatback rotational stiffness from the literature [12]. The dampers prevented the springs from thrusting the seatback forward in the rebound phase. The dampers were locked to the system only after the seatback rotation reached a target angle (18 degrees for the 17 km/h speed, 32 degrees for the 24 km/h speed) to restrict the damping effect to the rebound phase only. The constant stiffness of each of the two spring elements in both loading and unloading was defined as 13.5 kN/m per the specification in the tests. The damping constant of each of the two damper elements was determined as 2.5 kN/m-s^{-1} in tension through multiple iterations to represent the seatback rotation response in the rebound phase. The damping constant in compression was 0.0 kN/m-s^{-1}.

The seatbelt model consisted of two-dimensional seatbelt elements over the occupant and one-dimensional seatbelt elements at the shoulder and lap anchorage points. The "seatbelt" material type in LS-Dyna, which was validated against an elongation test of a generic seatbelt, was selected for the seatbelt model. The seatbelt webbing with two-dimensional elements was fitted over the occupant, which was positioned in a target posture and settled on the seat cushion. In the tests, an initial belt tension of 26.7 N was applied on the shoulder belt and a tension of 17.8 N was applied on the lap belt. In the model, the tension was applied at each end of the one-dimensional seatbelt elements from the beginning of the impact until the HBM started pulling the seatbelt, which was about 50 ms.

Human Body Models

The GHBMC male 50th percentile detailed model (M50-O v4.5) and simplified model (M50-OS v2.0) were used in this study. The height and weight (1.75 m and 78.6 kg of M50-O and 1.75 m and 78.5 kg of M50-OS) were close to the averages of the eight PMHSs (1.76 ± 6.4 m and 78.4 ± 7.16 kg). The detailed HBM consisted of 1.26 M nodes and 2.19 M elements, while the simplified HBM consisted of 300 K nodes and 355 K elements. The detailed HBM is designed to simulate both human kinematics and tissue-level injury response, while the simplified HBM is designed to demonstrate similar kinematics to the detailed HBM in a shorter computational time. For the neck region, the detailed HBM has deformable cervical vertebrae, deformable discs (i.e. anatomical joints), flesh, skin, and 1D elements to represent muscles and ligaments, while the simplified HBM has rigid cervical vertebrae with zero-length beams (i.e. mechanical joints), flesh, skin, and 1D elements to represent muscles. Although the simplified HBM has other 1D elements in the neck for active musculature, the function was not used in this study because the biomechanical targets were generated from tests with PMHSs. For the thoracic spine, the vertebrae are deformable in the detailed HBM, but rigid in the simplified HBM. The thoracic vertebrae disc spaces are mechanical joints instead of anatomical joints in both HBMs. For the soft tissue in the back of the torso, the detailed HBM has anatomically-accurate muscle groups as well as a layer of 3D elements representing the subcutaneous tissue, while the simplified HBM has a single 3D part to represent both the subcutaneous tissue and muscle groups.

Positioning of the HBMs was determined in terms of eight parameters. Figure 2 illustrates the definitions of the parameters, which were the only available information about the PMHS postures in the tests. Positioning limbs was achieved through a limb positioning function in a pre-processor for the simplified HBM and through multiple steps of positioning simulation for the detailed HBM. In the positioning simulations, each limb was rotated around a corresponding joint by applying a prescribed motion while deformation of the other body regions was constrained. This method was also applied to rotating the head of the simplified HBM around the occipital condyle joint in the sagittal plane to make the Frankfort plane horizontal since the limb positioning function was not available at the occipital condyle joint. Placing the HBM on the seat cushion foam was achieved through a seating simulation, where gravity was applied to the HBM until it settled on the seat. Table I lists values of each parameter for the HBMs at the end of the seating simulations and the averages of the PMHSs. All values were close to the averages and/or within the standard deviations of the PMHSs. The HBM horizontal relative distance to the seatback pivot was rather close to the upper boundary of those of the PMHSs to allow a reasonable margin that the seatback cushion foam could fill in. The target relative distances between the HBM head and the head restraint were achieved by adjusting the location of the head restraint as in the PMHS tests. The HBM hands were placed on each side of the thighs without any restraints. In the PMHS tests, the thumbs were tied with a single thin string.

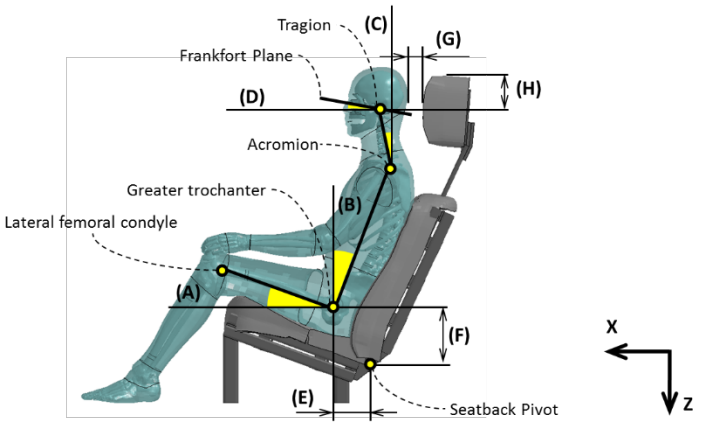

Fig. 2. Positioning parameters of HBM and PMHS: (A) thigh angle, (B) torso angle, (C) neck angle, (D) head angle, (E) horizontal, (F) vertical distance between the greater trochanter and the seatback pivot, (G) horizontal distance between the head and the head restraint front, and (H) vertical distance between the tragion and the head restraint top.

TABLE I

POSITIONING PARAMETERS OF EACH HBM AND THE AVERAGE OF THE EIGHT PMHSS IN THE SLED TESTS

	Detailed HBM	Simplified HBM	PMHS
(A) Thigh angle	16.1	17.2	15.3 ± 3.7
(B) Torso angle	23.0	23.1	22.5 ± 6.5
(C) Neck angle	10.0	9.0	10.8 ± 8.5
(D) Head angle	0.1	-0.6	0 ± 1
(E) Hip x-distance from the seat	175.1	176.2	154.0 ± 34.9
(F) Hip z-distance from the seat	184.5	193.5	195.6 ± 18.4
(G) Head x-distance from the head restraint	50.0	53.4	50 ± 5
(H) Head z-distance from the head restraint	105.6	106.6	105 ± 5

Biofidelity Evaluation

Measurements listed in Table II were collected in a sampling frequency of 12.5 kHz and filtered according to SAE J211, as in the tests, to be correlated with the PMHS biomechanical response targets. In the PMHS tests, data from head instrumentation (6aω) were transformed to the centre of gravity, and data from the spine and pelvis instrumentation (3aω) were measured in the local coordinate system at the superior edge of the vertebral body for T1, and at the spinous process for T12 and S1 [8]. The measurements on the HBMs were at the centre of gravity in the local coordinate of each body region or bone structure.

The biofidelity of the HBMs was evaluated by the NHTSA Biofidelity Ranking System (BRS) in terms of two aspects: internal and external biofidelity [10]. External biofidelity is intended to describe parameters measuring how much like a human the surrogate loads the vehicle, while internal biofidelity is intended to describe parameters measuring how much like a human the surrogate responds to the crash. Occipital condyle load was eliminated from the list because the simplified HBM has not been designed to measure it. HIC15 and the time when the head contacted the head restraint front face were excluded from the internal biofidelity evaluation because it could duplicate evaluating the head kinematics. The seat pan load was also excluded because the methodology of impact simulations in this study was unable to provide tension loads due to a lack of considering the initial compression by the occupant weight. The force on the lap belt was not a part of the biomechanical targets because of its large standard deviation in the PMHS tests [8].

Though the biofidelity of HBM is commonly evaluated by CORrelation Analysis (CORA) [14], this study used BRS for two reasons: the BRS evaluation is objective as well as quantitative; and it was used for ATDs with the same experimental system as the PMHS tests, where Hybrid III, BioRID II and RID3D were evaluated [11]. In the tests, the BioRID, which is the current standard rear-impact ATD, was most biofidelic due to its articulated spine having the same number of vertebrae as humans, and the Hybrid III, which is the current standard frontal impact

ATD, was least biofidelic due to its rigid spine box [11]. To compare time histories of each measurements, BioRID was selected due to its highest biofidelity among the tested ATDs. The scores from the ATD tests were used to compare with the HBM to examine its biofidelity relatively.

The BRS evaluates biofidelity of occupant surrogates with one overall score or rank, B, based on multiple measurements within multiple body regions and/or test conditions, as shown in Equation 1:

$$B = \frac{\sum_i^l \left[\frac{\sum_j^m \left[\frac{\sum_k^n \sqrt{R_{i,j,k}}}{n} \right]}{m} \right]}{l} \quad (1)$$

Where *B* is biofidelity rank, *R* is response measurement comparison value, *i* is body region, *j* is test condition, *k* is response measurement, *l* is number of *i*, *m* is number of *j*, and *n* is number of *R*.

The *R* values can be determined by Equation 2:

$$R = \frac{\sum\{D(t)-C(t)\}^2}{\sum\{S(t)-C(t)\}^2} \quad (2)$$

Where *D* is dummy response, *C* is mean PMHS response, and *S* is mean PMHS response with upper or lower tolerance. In this study, all $\sqrt{R}$ values were calculated from the beginning of the impact till the end of the simulation (250 ms).

The $\sqrt{R}$ values indicate absolute deviation from the standard deviation. A value of $\sqrt{R} < 1$ means that the measured response is less than one standard deviation different from the mean target. In this study, BRS scores under 1.0 were regarded as "Good", BRS scores between 1.0 and 2.0 were regarded "Intermediate", and BRS scores above 2.0 were regarded as "Poor". Sensitivity of the total biofidelity score as well as each individual *R* value have been defined as 0.2, meaning that if there is a difference between two surrogates that is greater than 0.2, the biofidelity between the two surrogates is significantly different [10].

TABLE II
SELECTION OF MEASUREMENTS FOR THE BIOFIDELITY ANALYSIS

	BioRank Evaluation	**Measurements**
Internal	Head kinematics	Acc. X
		Acc. Z
		Rotation Y
	T1 kinematics	Acc. X
		Acc. Z
		Rotation Y
	Head to T1 kinematics	Rotation Y
	T12 Kinematics	Acc. Resultant
	Pelvis Kinematics	Acc. Resultant
		Rotation Y
External	HR front top and bottom Load	Normal force
	SB top, centre and bottom Load	Normal force

III. RESULTS

Both HBMs showed generally similar gross kinematics to the PMHS tests (Fig. A-2 in Appendix). As the sled buck moved forward, the occupant torso pushed the seatback rearward. The seatback rotation angle in the HBM simulations closely tracked the PMHS tests mean and standard deviation curves (Fig. 3). As the occupant ramped up the seatback, the pelvis and thighs lifted off from the seat pan. The lap belt restrained the pelvis and thighs throughout the events, but the shoulder belt loosened its contact over the torso as the torso leaned backwards

while the D-ring remained at the same location. The occupant contacted the head restraint with the neck first and the head later. The PMHS showed the neck interaction with the bottom of the head restraint more than the HBMs. Only at the 24 km/h speed, the occupant showed sufficient ramping up motion along the seatback, then the head wrapped around the top of the head restraint. The HBMs flexed the thighs at the end of the impact at the 24 km/h speed, while none of the eight PMHSs showed these kinematics. In the PMHS tests, the upper extremity translated with the whole body and then moved over the torso as the seatback reached the maximum angle. The simplified HBM extended the upper extremity, while the detailed HBM kept the upper extremity at the same position relative to the torso throughout the events.

For all comparison plots in this paper (Fig. 3-22), the detailed HBM is denoted with blue lines, the simplified HBM with red lines, the BioRID with grey lines, and the PMHS biomechanical targets with black lines (solid lines are the mean curves and dotted lines are the standard deviation boundaries). The $\sqrt{R}$ values from all biofidelity measurements are provided in Table A-I in Appendix.

Internal Loads

The measurements of head centre of gravity are shown in Fig. 4-6. The time when the back of the head contacted the front surface of the head restraint, which is indicated on the horizontal time axis in the figures, was 119 ms for the detailed HBM and 115 ms for the simplified HBM (113 ± 7.4 ms in the PMHS tests) at the 17 km/h speed and 114 ms for the detailed HBM and 113 ms for the simplified HBM (124.3 ± 11.5 ms in the PMHS tests) at the 24 km/h speed. The values of HIC15 are shown in a table inside the figure of head x-acceleration (Fig. 4). At both speeds, the HBMs and the BioRID showed a steeper increase of head x-acceleration after the initial contact with the head restraint. While the BioRID showed a higher peak x-acceleration than the mean value in the PMHS tests, both HBMs showed a smaller peak x-acceleration. The duration in both HBM simulations was longer than that of the PMHS tests, which primarily contributed to larger HIC15 values than the PMHS tests. For the head z-acceleration, both HBMs showed a negative peak first around the time of the head contact followed by a positive peak, which was observed with the PMHS too, though the timing was off from the PMHS tests (Fig. 5). Both HBMs had $\sqrt{R}$ of "Intermediate" (1.0~2.0) for head, while the BioRID scored "Poor" (above 2.0) except the z-acceleration at the 24 km/h speed (Table A-I). All the HBMs and the BioRID scored better $\sqrt{R}$ values for head x-acceleration at the 24 km/h speed than at the 17 km/h speed, although larger deviations in the head restraint contact time as well as the peak time were observed at the 24 km/h speed. This was because the standard deviations around the peak x-acceleration in the PMHS tests were large, which made the denominator of $\sqrt{R}$ small. Regarding head y-rotation (Fig. 6), at both speeds the PMHS head remained close to the initial angle (~0 degrees) with a small amount of forward rotation until approximately 110 ms. In contrast, all the HBMs and the BioRID head never exhibited any forward rotation. The initiation of rearward rotation was around 40 ms for the BioRID, 70 ms for the simplified HBM, 75 ms for the detailed HBM, and 110 ms for the PMHS. All the HBMs and the BioRID showed the peak rearward rotation angle within the biomechanical targets at the 17 km/h speed, but lower than the lower boundary at the 24 km/h speed. Both HBMs scored "Good" for the head rotation at the 17 km/h speed and "Intermediate" at the 24 km/h speed, while the BioRID scored "Intermediate" at both speeds.

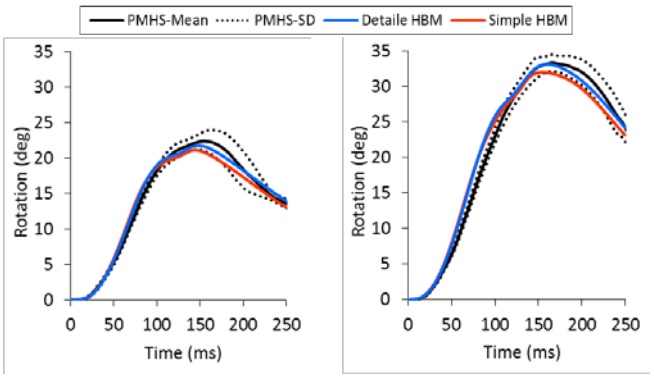

17 km/h 24 km/h

Fig. 3. Seatback rotation.

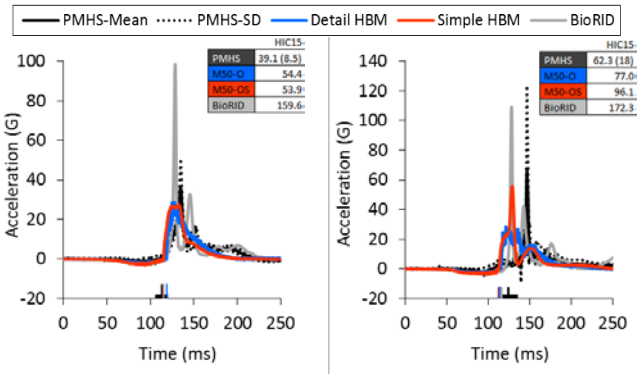

17 km/h 24 km/h

Fig. 4. Head x-acceleration.

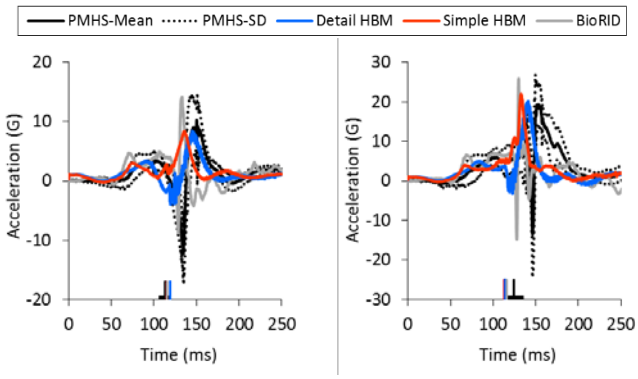

17 km/h 24 km/h

Fig. 5. Head z-acceleration.

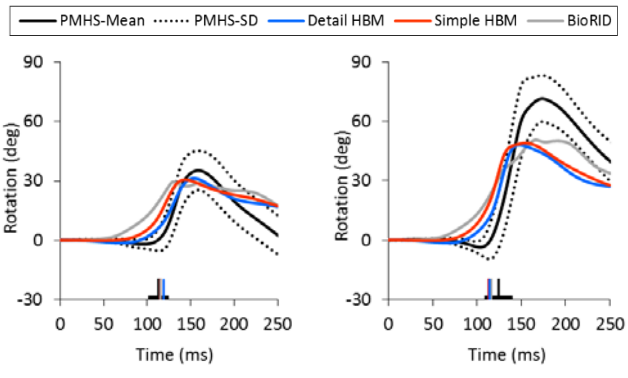

17 km/h 24 km/h

Fig. 6. Head y-rotation (sagittal).

The T1 x-accelerations at both speeds in the HBM simulations were similar in magnitude to the PMHS but slightly delayed in time (less than 10 ms), which become more apparent with the simplified HBM at the 24 km/h speed (Fig. 7). On the other hand, the BioRID showed the peak x-accelerations delayed in time at both speeds. For the T1 z-acceleration, all the HBMs and the BioRID failed to show the first positive spike observed with the PMHS at both speeds (Fig. 8). Both HBMs scored $\sqrt{R}$ of "Intermediate" for T1 accelerations except the z-acceleration at the 17 km/h speed (Table A-I). The BioRID exhibited $\sqrt{R}$ of "Poor" for the x-direction and "Intermediate" for the z-acceleration at both speeds. For the T1 y-rotation the BioRID tracked the lower bound of the biomechanical target throughout the event and received the best $\sqrt{R}$ values at both speeds (Fig. 9). The HBMs showed very similar response to each other with $\sqrt{R}$ of "Intermediate", but the scores were better at the 17 km/h speed.

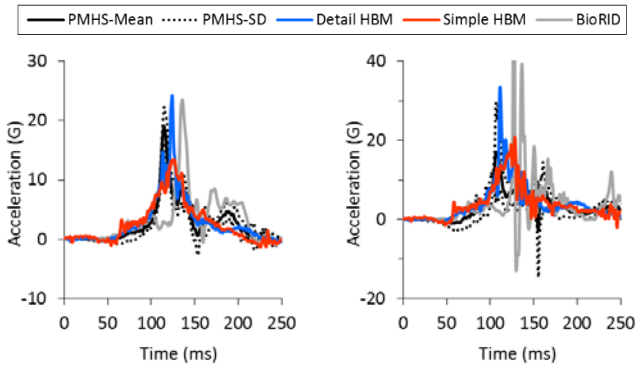

17 km/h 24 km/h

Fig. 7. T1 x-acceleration.

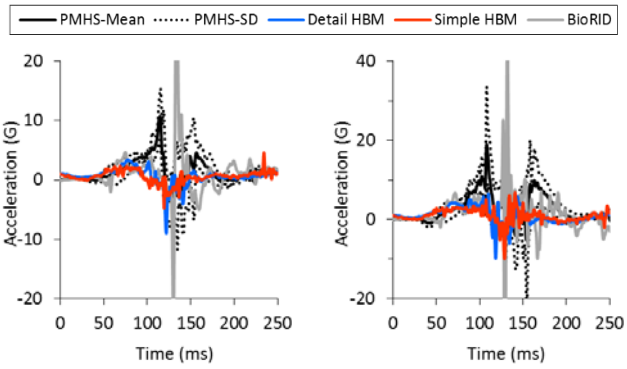

17 km/h 24 km/h

Fig. 8. T1 z-acceleration.

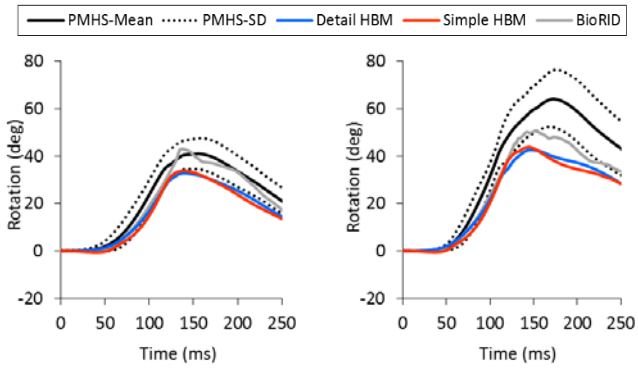

17 km/h 24 km/h

Fig. 9. T1 y-rotation (sagittal).

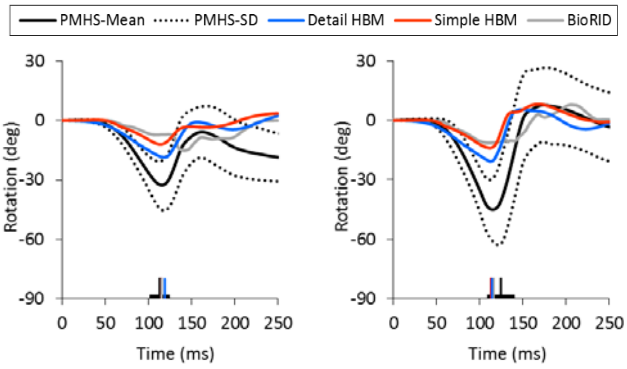

17 km/h 24 km/h

Fig. 10. Head y-rotation (sagittal) relative to T1.

For the head y-rotation relative to T1, the PMHS showed a large amount of relative forward rotation of the head (neck flexion) followed by relative rearward rotation (neck extension), and the amount of rotation increased with increasing impact severity (Fig. 10). All the HBMs and the BioRID showed this behaviour in similar timing, but the amount of rotations was much less than the PMHS and remained similar with increasing impact severity. Besides the PMHS, the magnitude of peak forward rotation was largest for the detailed HBM followed by the simplified HBM and then the BioRID. All the HBMs and the BioRID scored $\sqrt{R}$ of "Good" except the simplified HBM at the 17 km/h speed, and the detailed HBM received the best score.

For the T12 and pelvis resultant accelerations, both HBMs showed similar responses in both magnitude and timing to the PMHS, but the simplified HBM showed multiple large spikes throughout the event (Fig. 11-12). The detailed HBM received "Intermediate", while the simplified HBM received "Poor" (Table A-I). The BioRID corresponded with the biomechanical targets well and received the best $\sqrt{R}$, which was "Good" for the T12 acceleration at the 17 km/h speed and "Intermediate" for the rest. For the pelvis y-rotation, the PMHS exhibited a large deviation at both speeds and similar magnitude with increasing impact severity (Fig. 13). At both speeds, all the HBMs and the BioRID showed responses within the biomechanical targets and received $\sqrt{R}$ of "Good" (Table A-I). However, the HBMs did not show the rebound rotation observed with the PMHS. For the lap belt force, which was not included in the biomechanical targets from the PMHS tests, all the HBMs and the BioRID corresponded to the PMHS boundaries generally well (Fig. 14). However, the force at the end of the event increased at the 24 km/h speed unlike the PMHS which reduced to zero.

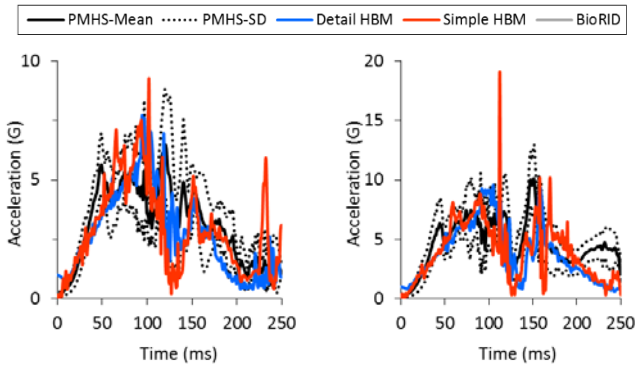

17 km/h 24 km/h

Fig. 11. T12 resultant acceleration.

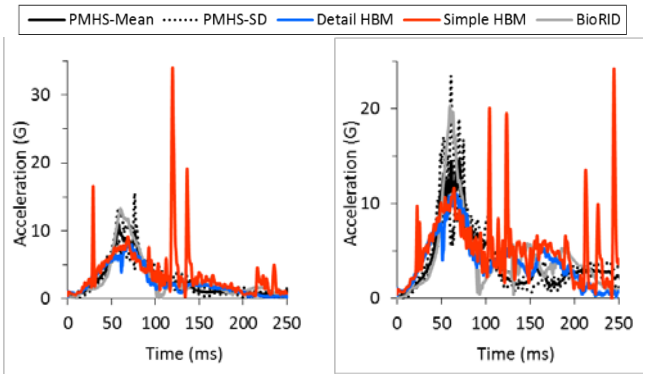

17 km/h 24 km/h

Fig. 12. Pelvis resultant acceleration.

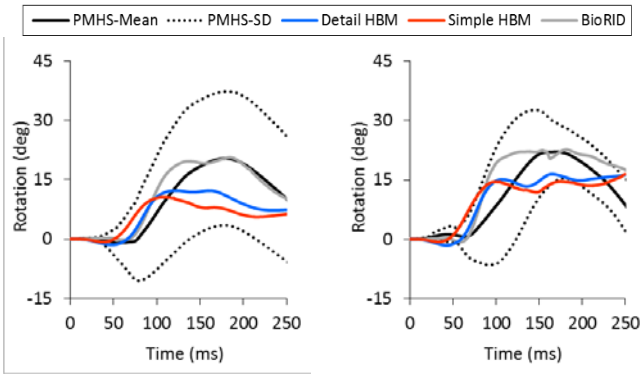

17 km/h 24 km/h

Fig. 13. Pelvis y-rotation (sagittal).

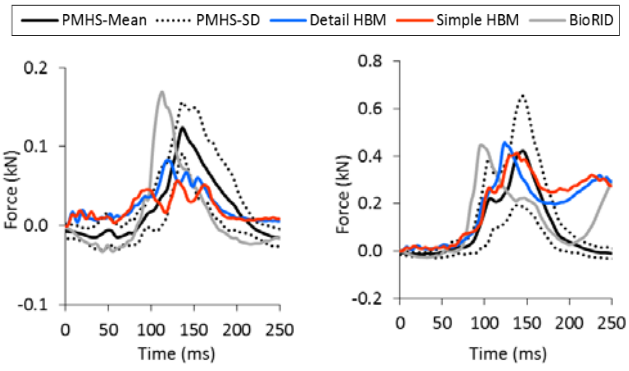

17 km/h 24 km/h

Fig. 14. Lap belt force.

External Loads

At both speeds, the HBMs and the BioRID showed a steeper increase of the head restraint front top load after the head contacted the head restraint (Fig. 15). In contrast to the top load, the HBMs and the BioRID showed smaller bottom loads than the lower boundary at both speeds (Fig. 16). The detailed HBM received better $\sqrt{R}$ scores than the simplified HBM at both speeds (Table A-I).

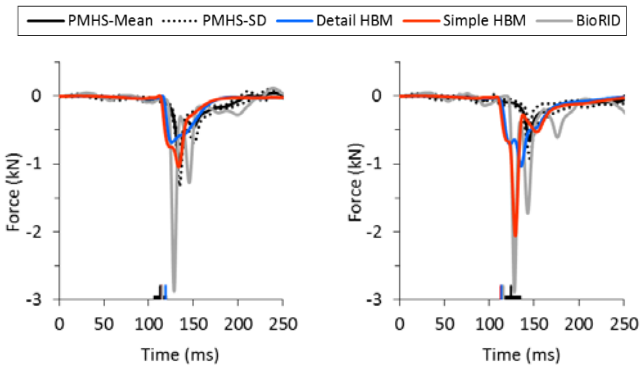

17 km/h 24 km/h

Fig. 15. Head restraint front top load.

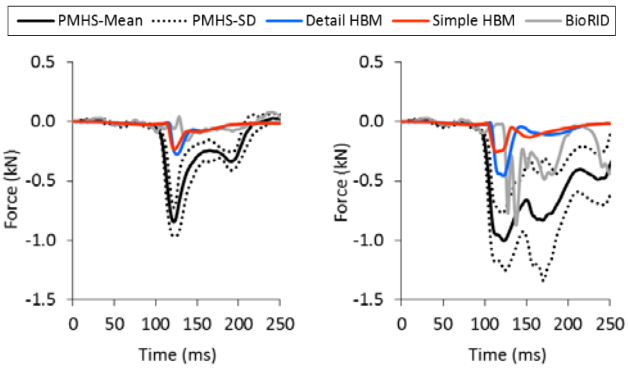

17 km/h 24 km/h

Fig. 16. Head restraint front bottom load.

For the seatback loads, all the HBMs and the BioRID corresponded to the biomechanical targets better at the 17 km/h speed than at the 24 km/h speed (Fig. 17-20). For the centre load at both speeds, the detailed HBM and the BioRID showed similar timing of the peak and time duration to the PMHS, while the simplified HBM showed the peaks early in time and with shorter time duration (Fig. 18). The BioRID corresponded to the peak load in the total load very well at both speeds (Fig. 20). In contrast, the total load for the detailed HBM did not increase with increasing impact severity as much as the PMHS and BioRID exhibited. At both speeds, the simplified HBM showed smaller total load than the lower boundary. The distribution of loads over the three load cell locations varied among the HBMs and the BioRID. The BioRID had higher loads at the top, while the HBMs distributed the loads at the bottom more. The BioRID received $\sqrt{R}$ of "Good" for seatback total load at both speeds (Table A-I). Both HBMs scored $\sqrt{R}$ of "Intermediate" for all load cells at both speeds except for the bottom at the 24 km/h with the simplified HBM. At both speeds, the detailed HBM scored better for the bottom loads, and the simplified HBM scored better for the centre and top.

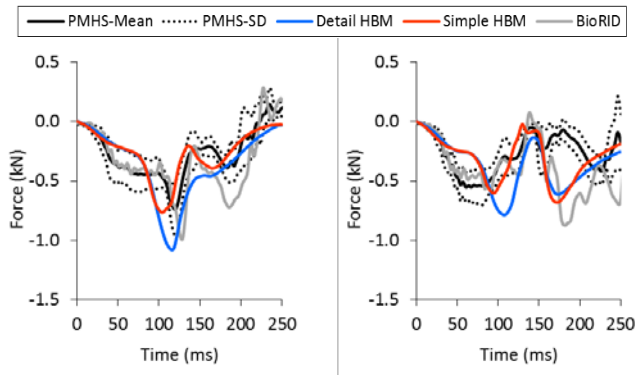

17 km/h 24 km/h

Fig. 17. Seatback top load.

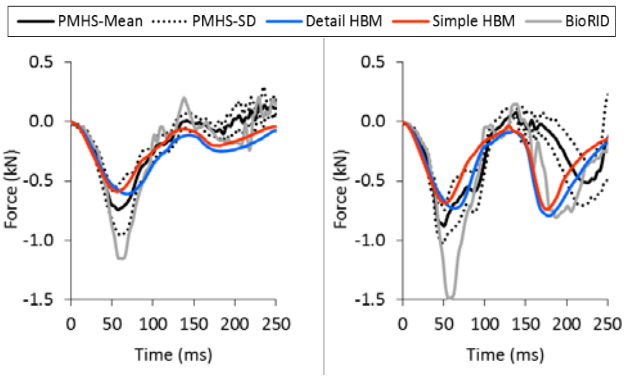

17 km/h 24 km/h

Fig. 18. Seatback centre load.

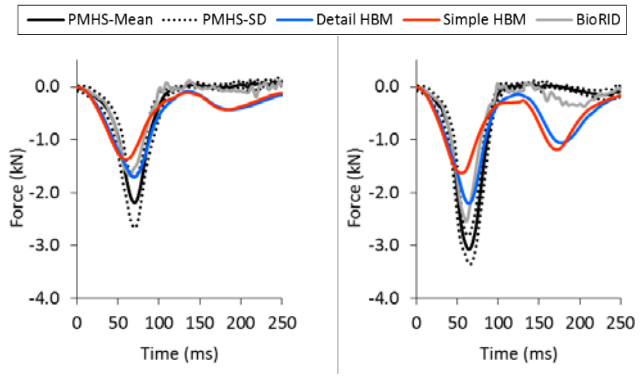

17 km/h 24 km/h

Fig. 19. Seatback bottom load.

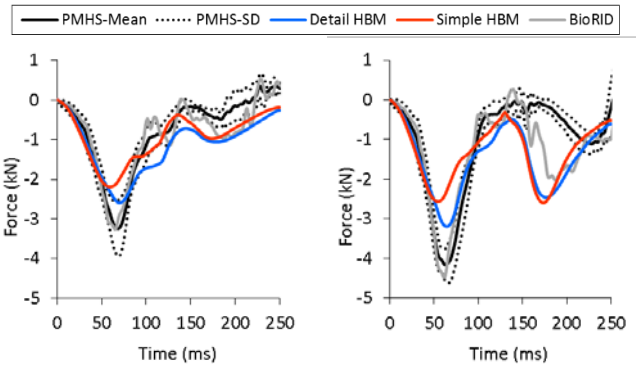

17 km/h 24 km/h

Fig. 20. Seatback total load.

The seat pan loads became negative (tension) first as the compression from the occupant was removed for the PMHS and the BioRID (Fig. 21-22). On the other hand, the HBMs failed to show this response. It was because the initial compression load was not considered in the simulations. It should be noted that the total seat pan compression load at the time when the HBM completed settling on the seat in the seating simulation was around 0.7 kN, which was similar to the total tension load when the PMHS initial compression load was removed. In the middle of the event (50-150 ms), the seat pan was compressed again for all the PMHS, the BioRID, and the HBMs. However, the second compression was removed earlier for the HBMs than the PMHS and the BioRID.

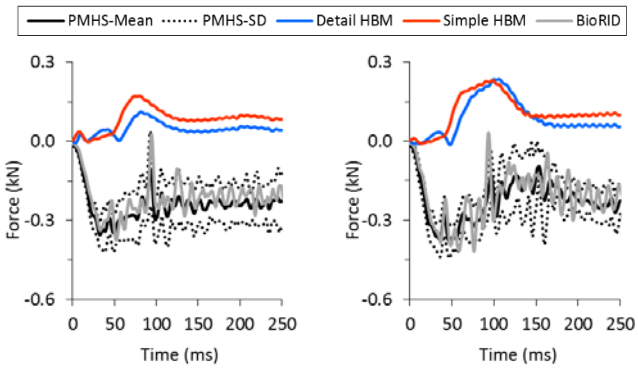

17 km/h 24 km/h

Fig. 21. Seat pan front load.

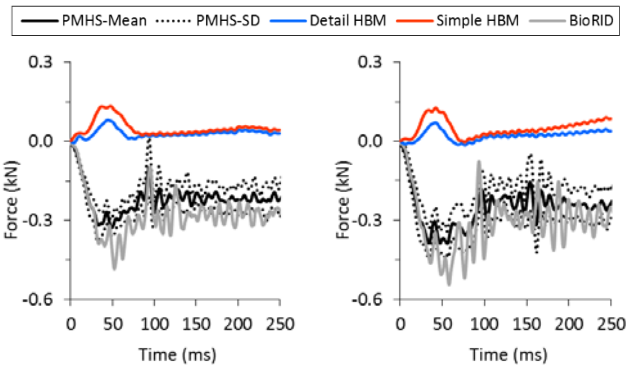

17 km/h 24 km/h

Fig. 22. Seat pan rear load.

Biofidelity Summary

Comparison of BRS scores of the HBMs, the BioRID II, the RID3D, and the Hybrid III [11] are shown in Fig. 23. Each BRS score is the average of $\sqrt{R}$ values for all response measurements in each component at both speeds per Equation 1. For the internal biofidelity, the detailed HBM received the best biofidelity in four out of five components (head, T1, head-T1, Pelvis) as well as in total. Only the detailed HBM achieved "Good" rating for the head-T1 rotation among the five occupants. The simplified HBM exhibited better or equivalent scores than the ATDs at head, T1 and head-T1, but worse scores at T12 and pelvis ("Poor" and "Intermediate", respectively) resulting in the lowest biofidelity in total. Both HBMs exhibited poorer scores than the ATDs in the two external biofidelity components except at the seatback for Hybrid III. In total, the detailed HBM received the third score after the BioRID and the RID3D, and the simplified HBM received the fourth score followed by the Hybrid III. Overall, the detailed HBM was ranked second behind the BioRID, and the simplified HBM was ranked lowest.

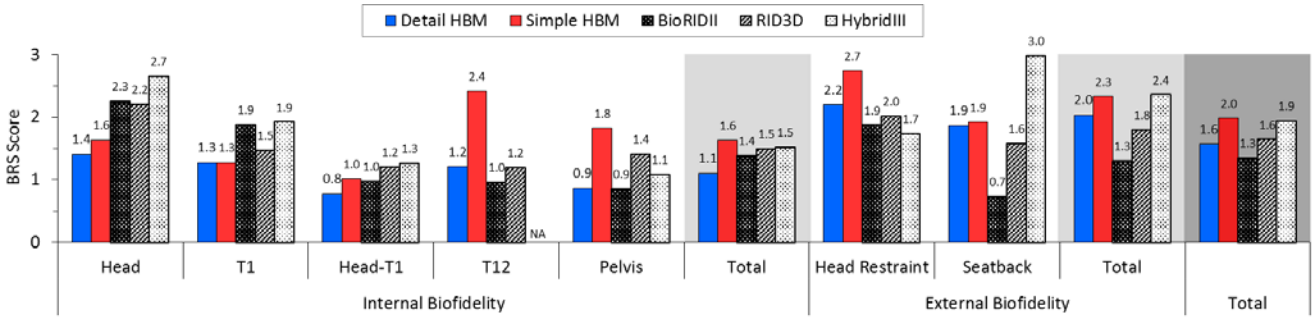

Fig. 23. Comparison of the biofidelity scores among the HBMs and the ATDs.

IV. DISCUSSION

Validity of the sled system model

The dynamic characteristics of the seatback reclining in the PMHS and ATD tests, which was primarily defined with stiffness of the springs and damping constant of the dampers, was represented well in this study. The seatback rotation responses at both speeds for both HBMs closely tracked the boundary curves in the PMHS tests. However, there were some slight differences observed. The model exhibited linear rebound (i.e. constant speed)

unlike nonlinear rebound in the tests. A specific value for the damping constant was unavailable in the tests, and the values in this study was determined through multiple iterations. A nonlinear damping constant might provide better representation of the seatback rotation response, especially in the rebound phase. During the preparation of the PMHS tests, a set of preliminary tests was conducted at the 24 km/h speed with a ballast of 40 kg attached to the seatback frame to evaluate the durability, repeatability and the reproducibility of the seatback rotation response. These evaluation tests can be used to validate modelling of the seatback spring-damper system if detailed information of the mass distribution on the seatback, which is critical for the response, was available. The ATD tests can be used to validate the sled system model at a system level. However, available FE models of ATDs were limited to the Hybrid III. However, the FE model was not validated under rear-impacts.

The methodology to provide the initial tension on the seatbelt was effective to represent the lap belt force response. In a simulation where the initial tension was not applied, the magnitude of the lap belt force did not increase as much as the simulations with the initial tension, which showed similar response to the PMHS tests.

Internal Biofidelity

The HBMs showed steeper increase and/or higher head x-acceleration compared to the PMHS. This trend was even more significant for the BioRID. This observation indicated that the HBMs and the BioRID contacted the head restraint more rigidly than the PMHS, likely due to difference in neck flexibility and head/skull compliance. The compliance of the head/skull was considered to be least for the BioRID followed by the simplified HBM, of which the skull is rigid, and then the detailed HBM. Additionally, around the time of head contact with the head restraint, the seatback rotation slowed down in the HBM simulations, while the seatback continued to rotate rearward in the PMHS tests. This also made the head acceleration as well as HIC15 higher with the HBMs compared to the PMHS. For the head y-rotation, at both speeds the PMHS head remained close to the initial angle with a small amount of forward rotation until approximately 110 ms. The detailed HBM showed this trend most closely followed by the simplified HBM, and then the BioRID.

The T1 x- and z-accelerations with the HBMs corresponded generally well at both speeds, while the BioRID showed multiple high spikes, likely due to a less compliant body structure around its T1 accelerometer. On the other hand, for the T1 rotation, the BioRID showed better agreement with the biomechanical targets than the HBMs at both speeds, likely due to difference in thoracic spine flexibility.

The head y-rotation relative to T1 was considered as an important component for the biofidelity of occupant surrogates in the rear-impact mode because of its relevance to rear-impact related injuries. All the HBMs and the BioRID showed smaller amount of the head-T1 relative rotation, which indicated less flexible necks/spines than the PMHS. Difference in the relative rotation among the HBMs and the BioRID was observed from the initial neck flexion phase (50 ms) until the head contact with the head restraint (115 ms), and biofidelity of the detailed HBM exceeded the other two occupants due to more biofidelic neck flexibility in the flexion direction. The difference in the extension direction cannot be discussed because the kinematics were restricted by the head restraint.

For the T12 and pelvis resultant accelerations, both HBMs showed similar responses to the PMHS, but the simplified HBM showed multiple large spikes throughout the event, likely due to less compliant T12 and pelvis in the simplified HBM. The thoracic spine vertebrae and pelvic bones in the simplified HBM are rigid, but deformable in the detailed HBM. For the pelvis y-rotation, while all the HBMs and the BioRID showed responses within the biomechanical targets, the HBMs did not show rearward rotation as well as rebound rotation as much as the BioRID did. This was likely due to the HBMs having stiffer thoracolumbar spine than the BioRID and stiffer soft tissue over the pelvis compared to the PMHS. The BioRID, which also has a stiffer pelvis region compared to the PMHS, showed larger pelvis rotation than the HBMs, likely due to difference in flexibility of the thoracolumbar spine. The HBMs' fixed pelvis kinematics and flexed thighs kept the lap belt engaged with the pelvis and caused the increase of lap belt force at the end of the events.

In total, the detailed HBM exhibited the best biofidelity in terms of kinematics from head to T1 followed by the simplified HBM, and then the BioRID. On the other hand, the BioRID demonstrated the best biofidelity in terms of kinematics from T1 to pelvis followed by the detailed HBM, and then the simplified HBM. These indicated that the HBMs have more flexible necks/spines but stiffer thoracolumbar spines than the BioRID in the rear-impact mode. This makes sense considering that the HBMs have been validated in the rear-impact mode at the neck body-regional level but never at the full-body level. Additionally, both HBMs showed better agreement with the biomechanical targets at the 17 km/h speed, which is consistent with the neck body-regional validation being

performed at lower speed (below ΔV of 15 km/h).

The effect of restraining the thumbs was not examined in this study. However, the differences in the upper extremity kinematics between the HBMs and the PMHS were more likely due to the initial position of the upper extremity, the characteristics of the upper extremity joints, and surrounding soft tissue elements, which restrict the upper extremity motion. In the PMHS tests, the thumbs were tied with a single thin string, which was broken during the tests. The PMHS showed the upper extremity translating with the whole body and then moving over the torso as the seatback reached the maximum angle, which suggested that effects of the thin string was negligible in terms of head and spine motions.

External Biofidelity

All the HBMs and the BioRID showed higher head restraint loads than the PMHS. As discussed about the head kinematics, the less flexible neck and less compliant head/skull caused the difference. The HBMs and the BioRID showed more disproportionate loads on the top of the head restraint compared to the PMHS. This was because the PMHS had more neck interaction with the head restraint than the HBMs and the BioRID. This is consistent with the observation that the HBMs and the BioRID have less flexible thoracolumbar spines than the PMHS resulting in less ramping up motion of the upper body.

For the seatback loads, the BioRID showed the best agreement with the biomechanical targets followed by the detailed HBM, and the simplified HBM. In the ATD tests, the BioRID, which had the most flexible spine among the three ATDs, showed smaller loads [11]. From the internal biofidelity measurements, the HBMs were considered to have less flexible spines than the BioRID. However, the HBMs exhibited smaller loads on the seatback. Not only the flexibility of the spine, but other factors that contribute to the total compliance for the interaction between the HBM and the seatback need to be investigated. The material properties and geometries of the cushion foam of the head restraint, seatback, and seat pan in the tests, which directly affected the loads on the three components, were unavailable in this study.

For the seat pan loads, the HBM simulations did not show the unloading of the initial compression load due to the occupant seating. The total seat pan compression load in the HBM seating simulations was equivalent to the total tension load when the PMHS initial compression was removed. Thus, performing the seating simulation and crash simulation consecutively could achieve a similar response to the PMHS (Fig. A-4 in Appendix). Besides the initial compression, the HBMs showed re-compression loads in a shorter time duration compared to the PMHS and the BioRID. This was likely due to difference in the interaction of the knee with the seat pan, which primarily provided the second compression load. The high speed video did not capture the interaction completely, but the motion of the thighs indicated that the thighs and knees engaged the seat pan longer than in the HBM simulations. The geometry of the seat pan cushion, the length of the thighs, and the characteristics of the knee and acetabulum joints could affect this difference.

Biofidelity Summary

For the internal evaluation, the detailed HBM exceeded the simplified HBM and the three ATDs at every component except at T12 for the BioRID. The simplified HBM scored better than the ATDs at only head, T1, and head-T1. The results were somewhat aligned with the findings from the internal measurement plots that the HBMs exhibited more biofidelic neck/spine but less biofidelic thoracolumbar spine than the BioRID in the rear-impact mode. In total, the internal biofidelity BRS score was highest for the detailed HBM followed by the ATDs, and then the simplified HBM. The superiority of the detailed HBM was significant since the difference in the scores was more than 0.2. The poorer scores at T12 and pelvis for the simplified HBM overwhelmed its better scores at head, T1, and head-T1, which are relevant body regions for rear-impact-related injuries.

For the external evaluation, the detailed HBM was ranked third after the two rear-impact ATDs and ranked better than the simplified HBM. The simplified HBM was ranked slightly above the Hybrid III. As previously discussed about the external measurement plots, these results were affected by not only the HBMs themselves but also the sled system model, which was unable to be fully validated in this study.

Overall, the detailed HBM was ranked second after the BioRID but slightly above the RID3D, and the simplified HBM was ranked lowest slightly behind the Hybrid III. For the detailed HBM, the poorer scores from the external biofidelity evaluation overwhelmed the better scores from the internal biofidelity evaluation.

V. CONCLUSIONS

The biofidelity of the GHBMC detailed and simplified HBM were evaluated by performing numerical simulations to represent a set of moderate-speed rear-impact tests using PMHS, and comparing the results with biomechanical targets generated from the PMHS tests. The dynamic characteristics of the seatback reclining in the experimental seat system was reproduced well by the sled system model in this study. The HBMs exhibited gross kinematics observed in the PMHS tests generally well. The HBMs showed better biofidelity 1) at the lower speed than the higher speed, and 2) in the head to T1 region than the T1 to Pelvis region. These findings were consistent with the HBMs having been validated in the rear-impact mode only at the neck body-regional level at lower speed (below ΔV of 15 km/h). The detailed HBM exhibited better biofidelity than the simplified HBM in all studied measurements, which was consistent with the detailed HBM having more biofidelic anatomy and material properties. Limitations of the HBMs in terms of the biofidelity in the rear-impact mode were indicated in the modelling of the whole spine and its surrounding flesh.

VI. REFERENCES

[1] Jorlöv, S., Bohman, K., Larsson, A. (2017) Seating positions and activities in highly automated cars – a qualitative study of future automated driving scenarios. *Proceedings of IRCOBI Conference*, 2017, Antwerp.

[2] EEVC (2002) Ad-hoc group on cervical spine injuries, Working group 12 report, Document No. 157.

[3] U.S. Department of Transportation (2017) Automated Driving Systems 2.0: A Vision for Safety, 2017. Available at: https://www.nhtsa.gov/sites/nhtsa.dot.gov/files/documents/13069a-ads2.0_090617_v9a_tag.pdf. Accessed: September 30, 2017.

[4] Davidsson, J., *et al.* (1998) Human volunteer kinematics in rear-end sled collisions. *Proceedings of IRCOBI Conference*, 1998, Goteborg.

[5] Deng, B., Begeman, P. C., Yang, K. H., Tashman, S., King, A. I. (2000) Kinematics of human cadaver cervical spine during low speed rear-end impacts. *Stapp Car Crash Journal*, **44**: pp. 171–88.

[6] Kitagawa, Y., Yamada, K., Motojima, H., Yasuki, T. (2015) Consideration on Gender Difference of Whiplash Associated Disorder in Low Speed Rear Impact. *Proceedings of IRCOBI Conference*, 2015, Lyon.

[7] Östh, J., *et al*. (2017) A female head–neck model for rear impact simulations. *Journal of Biomechanics*, **51**: pp. 49–56.

[8] Kang, Y., *et al*. (2012) Biomechancial responses of PMHS in moderate-speed rear impacts and development of response targets for evaluating the internal and external biofidelity of ATDs. *Stapp Car Crash Journal*, **56**: pp. 105–70.

[9] Mallory, A., and Stammen, J. (2007) Comparative evaluation of rear impact dummies static seat interaction and dynamic testing. *National Highway Traffic and Safety Administration*, NHTSA Docket No. 2007-27986-19.

[10] Rhule, H., Moorhouse, K., Donnelly, B., Stricklin, J. (2009) Comparison of WORLDSID and ES-2RE biofidelity using updated biofidelity ranking system. *21st International Technical Conference on the Enhanced Safety of Vehicles*, 2009, Paper No.09-0563.

[11] Moorhouse, K., Donnelly, B., Kang, Y., Bolte, J. H., Herriott, R. (2012) Evaluation of the internal and external biofidelity of current rear impact ATDs to response targets developed from moderate-speed rear impacts of PMHS. *Stapp Car Crash Journal*, **56**: pp. 171–229.

[12] Molino, L. (1998) Determination of moment deflection characteristics of automobile seat backs. NHTSA Docket No. 1998-4064-26.

[13] Kang, Y., Moorhous, K., Stammen, J., Bolte IV, J. (2008) An Experimental seat for measuring external biofidelity in rear impacts and a new instrumentation technique for the cervical spine of PMHS. *Injury Biomechanics Symposium*, 2008, Columbus.

[14] Pipkorn, B., *et al*. (2018) Occupant Protection in Far-Side Impacts. *Proceedings of IRCOBI Conference*, 2018, Athens.

VII. APPENDIX

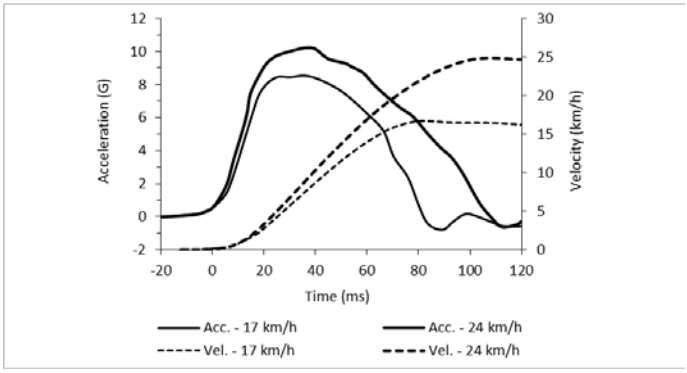

Fig. A-1. Sled pulses used in the PMHS tests and the HBM simulations.

Fig. A-2. Sequential motion of a PMHS (76.2 kg and 174.0 cm) in the tests (*top*), the detailed HBM (*centre*), and the simplified HBM (*bottom*).

TABLE A-I
BIOFIDELITY SCORES

		Detailed HBM		**Simplified HBM**		**BioRID** [11]	
		17 km/h	24 km/h	17 km/h	24 km/h	17 km/h	24 km/h
Internal	Head Acc. X	1.79	1.58	2.04	1.99	4.77	2.27
	Head Acc. Z	1.08	1.72	1.77	1.47	2.23	1.55
	Head Rot. Y	0.61	1.68	0.88	1.68	1.19	1.55
	T1 Acc. X	1.70	1.23	1.61	1.06	3.11	2.86
	T1 Acc. Z	0.92	1.00	0.97	1.02	1.19	1.74
	T1 Rot. Y	1.18	1.59	1.32	1.68	0.48	1.15
	Head to T1 Rot. Y	0.80	0.75	1.13	0.90	0.96	0.99
	T12 Acc. Res.	1.06	1.35	2.72	2.10	0.67	1.28
	Pelvis Acc. Res.	1.13	1.42	3.60	2.51	1.08	1.26
	Pelvis Rot. Y	0.38	0.51	0.57	0.62	0.24	0.85
External	HR – Top	1.55	2.85	1.93	4.51	2.09	1.66
	HR – Bottom	2.41	1.97	2.46	2.07		
	SB – Top	1.44	1.98	1.00	1.80	0.73	0.74
	SB – Centre	1.50	1.93	1.13	1.82		
	SB – Bottom	1.51	2.83	1.97	3.78		

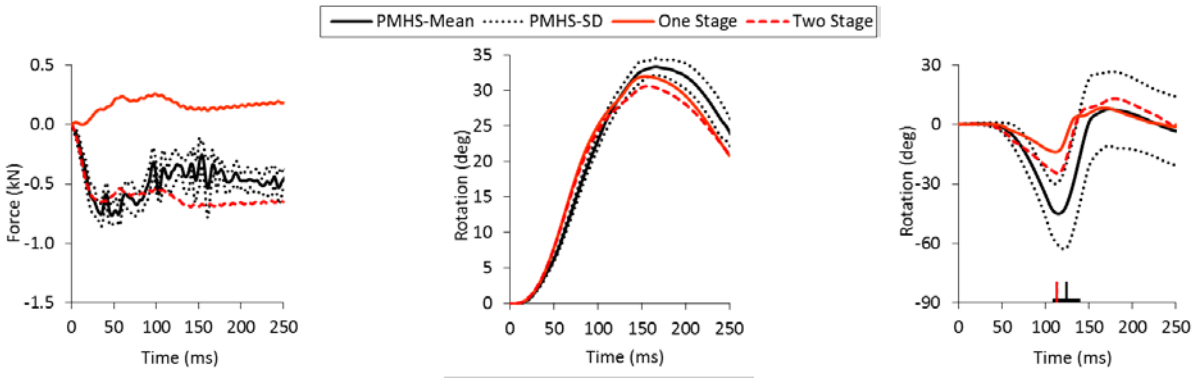

Total seat pan load | Seatback rotation | Head y-rotation relative to T1

Fig. A-4. Comparison of measurements between the impact-only (one-stage) and seating-impact (two-stage) simulations with the simplified HBM at the 24 km/h speed. In the two-stage simulation, first, only gravity was applied to the HBM until it settled on the seat, which took 170 ms. Consecutively, the impact pulse was applied to the sled buck for the duration of 250 ms as in the one-stage simulation. The HBM posture and the seatbelt fitting at the beginning of the impact stage were the same with those in the one-stage simulation. At the beginning of the impact stage, the contact between the HBM and the seatbelt webbing became active, and the initial tension of each side of the seatbelt was initiated for the duration of 50 ms as in the one-stage simulation. Each measurement from the two-stage simulation was subtracted by the value at the beginning of the impact stage. The two-stage simulation showed similar seat pan load to the PMHS tests (*left*). However, the seatback rotation (*centre*) and the occupant responses (*right*) also changed from the one-stage simulation. Further investigation on the simulation methodology is required.